CrossMark

RESEARCH PAPER

Characterization of phthalocyanine functionalized quantum dots by dynamic light scattering, laser Doppler, and capillary electrophoresis

Gonzalo Ramírez-García[1,2,3,4] · David O. Oluwole[5] · Siphesihle Robin Nxele[5] ·
Fanny d'Orlyé[1,2,3,4] · Tebello Nyokong[5] · Fethi Bedioui[1,2,3,4] · Anne Varenne[1,2,3,4]

Abstract In this work, we characterized different phtalocyanine-capped core/shell/shell quantum dots (QDs) in terms of stability, ζ-potential, and size at various pH and ionic strengths, by means of capillary electrophoresis (CE), and compared these results to the ones obtained by laser Doppler electrophoresis (LDE) and dynamic light scattering (DLS). The effect of the phthalocyanine metallic center (Zn, Al, or In), the number (one or four), and nature of substituents (carboxyphenoxy- or sulfonated-) of functionalization on the phthalocyanine physicochemical properties were evaluated. Whereas QDs capped with zinc mono-carboxyphenoxy-phtalocyanine (ZnMCPPc-QDs) remained aggregated in the whole analyzed pH range, even at low ionic strength, QDs capped with zinc tetracarboxyphenoxy phtalocyanine (ZnTPPc-QDs) were easily dispersed in buffers at pH equal to or higher than 7.4. QDs capped with aluminum tetra-sulfonated phthalocyanine (AlTSPPc-QDs) and indium tetra-carboxyphenoxy phthalocyanines (InTCPPc-QDs) were stable in aqueous suspension only at pH higher than 9.0 due to the presence of functional groups bound to the metallic center of the phthalocyanine. The ζ-potential values determined by CE for all the samples decreased when ionic strength increased, being well correlated with the aggregation of the nano-conjugates at elevated salt concentrations. The use of electrokinetic methodologies has provided insights into the colloidal stability of the photosensitizer-functionalized QDs in physiological relevant solutions and thereby, its usefulness for improving their design and applications for photodynamic therapy.

Keywords Colloidal stability · Quantum dots · Capillary electrophoresis · Photodynamic therapy · Phthalocyanines · Photosensitizers

✉ Fethi Bedioui
fethi.bedioui@chimieparistech.fr

✉ Anne Varenne
anne-varenne@chimie-paristech.fr

[1] Chimie ParisTech, PSL Research University, Unite de Technologies Chimiques et Biologiques pour la Sante UTCBS, 75005 Paris, France

[2] INSERM, UTCBS, U 1022, 75006 Paris, France

[3] CNRS, UTCBS UMR 8258, 75006 Paris, France

[4] Université Paris Descartes, Sorbonne Paris Cite, UTCBS, 75006 Paris, France

[5] Department of Chemistry, Rhodes University, Grahamstown 6140, South Africa

Introduction

Quantum dots (QDs) are inorganic semiconductor nanocrystals having unique optical properties such as high luminescent quantum yields, large molar extinction coefficients, tunable excitation and emission spectra, and photostability [1, 2]. Hence, they can be used as imaging and analytical probes for biomedical studies and as therapeutic systems in the nanomedicine field [3, 4].

In order to improve their biological applications, surface modification is crucial for providing biocompatible physicochemical properties and aqueous solubility and for preventing aggregation [1, 5]. Various types of nanoparticles (NPs), including QDs have been functionalized and proposed to be applied in photodynamic therapy (PDT) [6]. In this sense, a family of glutathione capped core/shell/shell QDs has been recently synthesized and covalently functionalized with phthalocyanines (Pc) containing different functional groups and metallic centers [7–9]. To facilitate the discussion, they will be denoted below as Pc conjugated QDs (Pc-QDs). They

Springer

have been characterized in terms of photophysical properties in order to be applied in photodynamic therapy, making the synthesized Pc-QDs viable and active photosensitizers.

These nanohybrids hold great promise in PDT because they can act as carriers of photosensitizers, energy donors to excite the photosensitizers, and as an imaging contrast agent. Their unique optical and emission properties have been precisely tuned in order to make it able to emit light in the excitation region of their corresponding Pcs, permitting the energy transfer via the Förster resonance energy transfer (FRET) mechanism, giving a theranostic tool for cancer detection and treatment.

However, one of the most important current limitations of PDT is that the majority of the photosensitizers have extended delocalized aromatic π electron systems, a characteristic property that allow them to absorb light efficiently. At the same time due to π-π stacking (attractive noncovalent interactions between aromatic rings, since they contain π bonds) and hydrophobic interactions, they easily form aggregates in aqueous media [10]; it is therefore necessary to evaluate their colloidal stability before biological applications.

In general, QDs are characterized in terms of particle size, size distribution, and morphology by using various analytical methods, such as transmission electron microscopy (TEM), scanning electron microscopy (SEM), dynamic light scattering (DLS), UV/vis absorbance and fluorescence spectroscopy, size-exclusion chromatography (SEC), and capillary electrophoresis (CE) [11–13].

CE has emerged as a powerful tool to separate and characterize different nanoparticles, among which QDs [13–21]. In comparison to the classical methods for NP physicochemical characterization, CE presents several advantages, such as high separation efficiency in aqueous, hydro-organic, or organic media, low sample and products consumption, simple sample preparation, accurate quantitative analysis, reduced analysis time, and a high degree of automation [22]. Different electrokinetic modes have been applied for NP characterization, including capillary zone electrophoresis (CZE), capillary gel electrophoresis (CGE), micellar electrokinetic chromatography (MEKC), and isotachophoresis (ITP) [16, 23]. The evaluation of the colloidal properties of nanoparticles in physiologically relevant buffers has also been carried out on the basis of their electrophoretic mobilities and diffusion patterns, which depend mainly on the charge-to-size ratios [12, 24].

The appropriate characterization of NPs, before in vitro or in vivo investigation, by means of complementary techniques is mandatory to predict their behavior in the living systems [25–27]. The surfaces of QDs have been continuously modified through binding of functional groups or molecules to provide stability, biocompatibility, selectivity, and functionality for biological applications [3, 28]. Particularly, the colloidal properties in physiologically relevant solutions are important from the formulation step before the administration, until the clearance by the organism. Currently, the colloidal stability

of the nanoparticles is a relevant challenge during the development of a new therapeutic nanomaterial.

In this work, Pcs were linked to the surface of QDs by means of covalent bounds in order to be applied for PDT. Glutathione (GSH) was chosen as the capping ligand for the QDs due to its unique chemical properties such as high electron donating capacity thanks to its sulfhydryl moieties, good antioxidant activity, stabilizer as well as its ability to be linked to other molecules via its sulfhydryl, amine, and carboxylic functional moieties [7]. For further understanding of the effects of different functional groups and the structure of the conjugates, complementary techniques (Doppler electrophoresis (LDE), DLS, CE, and Taylor dispersion analysis) were employed in order to evaluate their colloidal stability and physicochemical properties in buffered solutions at various pH and ionic strength ranges.

More precisely, a family of water-soluble QDs functionalized with various Pc (see experimental section for further details) was successfully synthesized and characterized by CE using physiologically relevant buffers as background electrolyte. The effect of the Pc metallic center (Zn, Al, or In), the number (one or four), and nature of substituents (carboxyphenoxy- or sulfonated-) of functionalization on the phthalocyanine physicochemical properties were tested. The purity and number of populations, colloidal stability, hydrodynamic size, and ζ-potential values of the Pc-QDs were determined by CZE and Taylor dispersion analysis (TDA) performed in the CE apparatus and compared with those obtained by classical techniques such as DLS and LDE. The characterization of the colloidal properties of this family of Pc-QDs in buffered solutions at physiological conditions allows for the determination of the optimal conditions for dispersion and applicability of these nanohybrids in biological systems.

Materials and methods

Reagents

Ultrapure water (≥18.2 MΩ) purified by Milli-Q system (Millipore, Bedford, MA, USA) was used for preparation of all solutions. Na_2HPO_4, NaH_2PO_4, rhodamine B (RB), 1-ethyl-3-(3-dimethylaminopropyl)-carbodiimide (EDC), N-hydroxyl succinimide (NHS), and GSH were purchased from Sigma-Aldrich, while $Na_2CO_3 \cdot 10H_2O$ and $NaHCO_3$ were obtained from Merck. NaOH (1.0 M) solution Normandose was purchased from VWR.

Buffer preparation

Buffers for dispersion and analysis were prepared at initial concentration of 150 mM and thereafter diluted as required. Appropriate ratios of Na_2HPO_4 and NaH_2PO_4 were used for

phosphate buffer solution (PB) preparation or $Na_2CO_3 \cdot 10H_2O$ and $NaHCO_3$ for sodium carbonate buffers (SCB). The buffers were filtered through a 0.20-μm filter before use.

Preparation of the phthalocyanine conjugated QDs

The family of glutathione capped-QDs was synthesized and covalently functionalized using previously reported procedures [7–9]. The phthalocyanines are linked to the GSH-QDs via an amide bond using the carboxyl or sulphonate groups of the former and the NH_2 group on the glutathione capping of the latter. The schematic structure of these glutathione capped-QDs conjugates with phthalocyanines is presented in Fig. 1. The corresponding Pc-QDs are the zinc mono substituted carboxyphenoxy phthalocyanine-GSH-CdTe/CdS/ZnS QDs [6.7 nm] (ZnMCPPc-QDs), zinc tetra substituted carboxyphenoxy phthalocyanine-GSH-CdTe/CdS/ZnS QDs [6.7 nm] (ZnTCPPc-QDs) [7], aluminum tetrasulfonated phthalocyanine-GSH-CdTe/CdS/ZnS QDs [6.6 nm] (AlTSPPc-QDs) [9], and indium tetracarboxyphenoxy phthalocyanine-GSH-CdTe/ZnSe/ZnO-QDs [6.2 nm] (InTCPPc-QDs) [8]. In the case of InTCPPc-QDs, ZnSe was employed for the first shell instead of CdS used in the initially reported ZnMCPPc-QDs, ZnTCPPc-QDs, and AlTSPPc-QDs due to the fact that CdS shell leads to increase in the amount of cadmium ion present in the complex unlike ZnSe which is relatively biocompatible [8]. The numbers in square brackets refer to the diameter of the crystalline structure of the nanoconjugates as obtained from X-ray dispersion (XRD) analysis. They were precipitated with excess methanol and purified before to be re-dispersed in the corresponding aqueous buffer solution.

Analysis and instrumentation

The hydrodynamic diameter (d_H) and ζ-potential of the Pc-QDs were initially calculated using DLS and LDE measurements, respectively, with a Malvern Zetasizer Nanoseries, Nano-ZS90. The hydrodynamic diameter was measured with an angle of 173° backscatter using 10 mm × 10 mm quartz cuvettes, whereas a disposable folded capillary cell was used for ζ-potential measurements. The assumption of a quantum dot refractive index of 2.550 [29] and a dispersant refractive index of 1.332 with a viscosity of 0.8872 cP was made consistently across all the dispersions. For size determination, the hydrodynamic diameter corresponds to scattering peak maxima as determined by intensity distributions, while the volume/number distributions where used to analyze the relative weight of each peak in the distribution (if multimodal). Electrophoretic separations were performed with a 7100 model Capillary Electrophoresis System (Agilent Technologies, Waldbronn, Germany). Fifty micrometers internal diameter × 45 cm fused silica capillaries (detection length: 21 and 36.5 cm for fluorescence and absorbance detections, respectively) from Polymicro Technologies (Phoenix, AZ, USA) were used after activation by successive flushes (925 mbar) with 1.0 M NaOH (15 min), 0.1 M NaOH (15 min), and H_2O (5 min), respectively. The capillary cartridge was set at a temperature of 25 °C. The detection wavelength used with a diode array detector (DAD) was 200 nm, and >520 nm for fluorescence detection (FD) (excitation source 480 nm). The external module Picometrics Zetalif LED connected by fiber optical to the CE system was used for LED-induced fluorescence detection.

For electrophoretic studies, injections were performed hydrodynamically by applying a pressure of 20 mbar at the capillary inlet for 10 s. Successive injection zones were performed in the following order: neutral marker, particle sample, and electrophoretic buffer. Rhodamine B (200 μM) was used as a neutral fluorescent marker (pKa value of 3.22 [30]), allowing for electroosmotic flow (EOF) measurement. The applied voltage was +14 kV. Pc-QDs were separated in bare fused silica capillaries after a preconditioning sequence of successive flushes (925 mbar) of 0.1 NaOH (2 min), water (2 min), and finally BGE (3 min). Electrophoretic mobility of the Pc-QDs was obtained from the migration time measured at the mass barycenter of the electrophoretic profil. Each sample in this study was analyzed four times with the average result presented.

For TDA, once preconditioned, the inlet end of the capillary was transferred into the vial containing the NP suspension, and a pressure drop was applied (30 mbar). The TDA analysis was performed with front concentration profiles (and not pulse profiles) because this approach permits easy signal normalizations especially when the precise NP concentration is unknown and gives more accurate results as it involves less pressure step changes [19].

The numeric electrophoretic mobility values were obtained from the barycenter of CE and LDE profiles, allowing the calculation of the ζ-potential values thanks to the equation derived by Ohshima et al. and simplified by Pyell et al. [31]. Adequate mathematical models were also used to convert the taylorgrams into diffusion coefficient (Aris-Taylor equation) and then into an apparent equivalent sphere radius (r_H) via the Stokes–Einstein equation [19, 31–34].

Results and discussion

The photophysical characterization of the synthesized Pc-QDs has already been described [7–9]. For FRET to occur, there has to be an efficient overlap between the emission of the QDs (donor) and the Pcs (acceptor) spectra. As a summary of the photophysical properties of the analyzed Pc-QDs, we found that the QDs conjugates with ZnMCPPc and ZnTCPPc show maximum emission wavelength (λ_{emi}) at 630 nm, while the

Fig. 1 Schematic representation of the phthalocyanine capped GSH-QDs nanoconjugates. *ZnMCPPc-QDs*, zinc mono substituted carboxyphenoxy phthalocyanine-GSH-CdTe/CdS/ZnS QDs; *ZnTCPPc-QDs*, zinc tetra substituted carboxyphenoxy phthalocyanine- GSH-CdTe/CdS/ZnS QDs; *AlTSPPc-QDs*, aluminum tetrasulfonated phthalocyanine-GSH-CdTe/CdS/ZnS QDs; *InTCPPc-QDs*, indium tetracarboxyphenoxy phthalocyanine-GSH-CdTe/ZnSe/ZnO-QDs
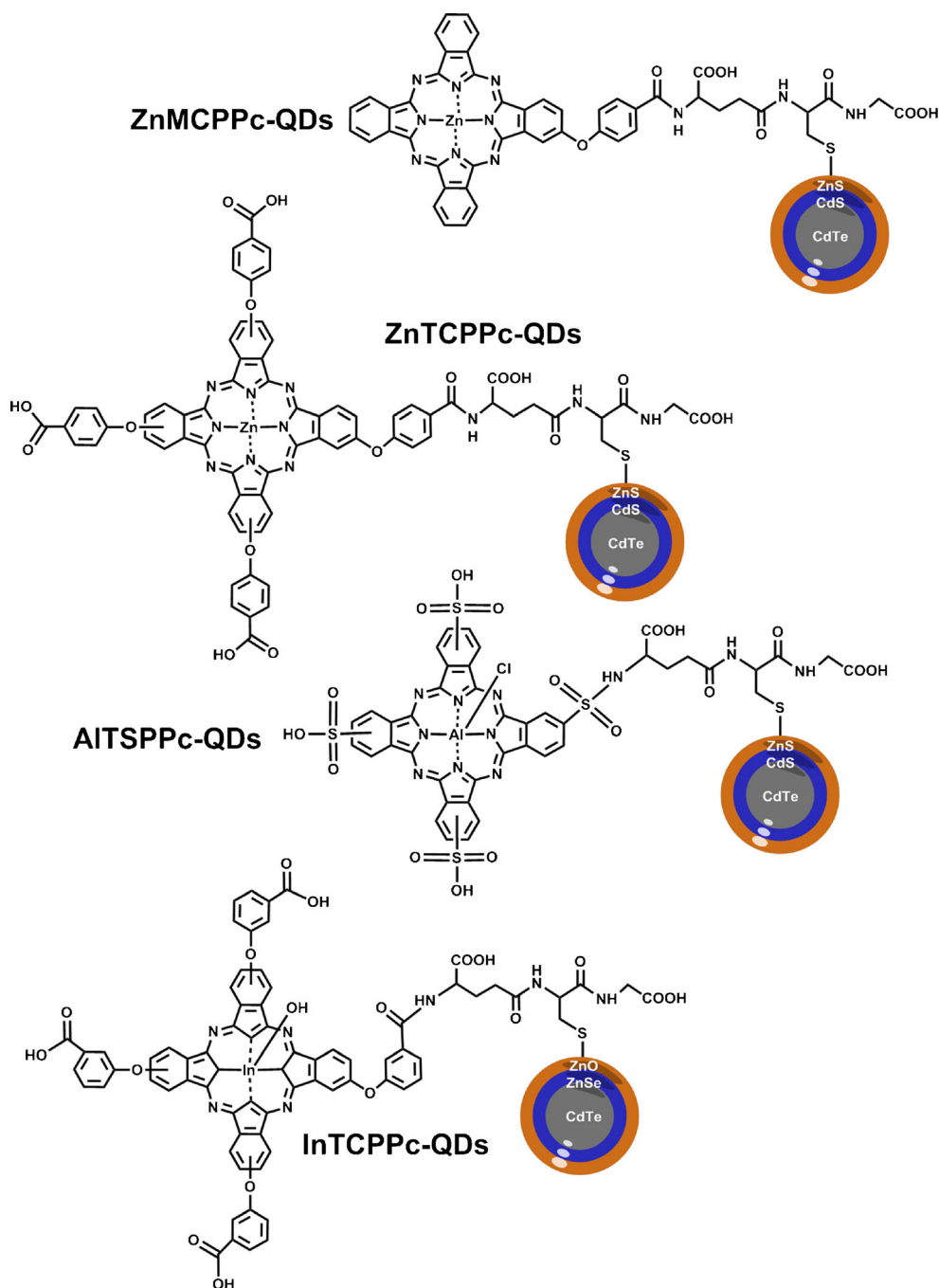
maximum absorption wavelength (λ_{abs}) of the corresponding conjugates was at 675 and 681 nm, respectively. The corresponding FRET efficiency (E_{ff}) was 97% for ZnMCPPc-QDs and 98% for ZnTCPPc-QDs, with fluorescence lifetimes (τ_F) of 3.0 and 2.9 ns, and fluorescence quantum yields (Φ_F) of 0.19 and 0.12, respectively [7]. The InTCPPc-QDs presented a λ_{emi} of 599 nm, while the corresponding conjugate presented a λ_{abs} of 689 nm, thus resulting in a 71% E_{ff}. Their τ_F and Φ_F were 4.9 ns and 0.014, respectively [8]. Finally, for AlTSPPc-QDs, the QDs presented a λ_{emi} of 626 nm, while the conjugate presented a λ_{abs} of 674 nm, giving as a result a

93% E_{ff}. In the latter case, their τ_F and Φ_F values were 3.3 ns and 0.006, respectively [9].

Before analysis, the synthesized Pc-QDs were initially dispersed in the corresponding buffer and then gently sonicated by using a conventional sonication bath. All modified Pc-QDs presented different colloidal stability properties. A clear aggregation of all the Pc-QDs was observed at pH lower than 6.5. Independently to the size values determined by means of instrumental measures (described below), Pc-QDs modified with tetra substituted phthalocyanine were better dispersed by sonication compared to the mono substituted conjugates.

This might be due to the absence of functional groups on the Pc and the consequent decrease in charge density and thereby in electrostatic repulsions.

Figure 2 shows the electropherograms of the ZnTCPPc-QDs, their precursors, and the synthesis reactants in 15 mM phosphate buffer (pH 7.4). The ZnTCPPc-QDs electrophoretic profile presents a main peak (peak 6) associated to other small peaks. Peaks 1, 2, and 3 can be attributed to the EOF marker (injected in all the analysis), NHS, and GSH, respectively. Only a small peak that may correspond to GSH-QDs residues was visualized in the ZnTCPPc-QDs profile (peak 4), indicating almost a total consumption for ZnTCPPc-QDs functionalization. The superposed peak 5 on peak 6 could be due to an excess of free tetra substituted carboxyphenoxy phthalocyanine (ZnTCPPc). The small signal around -1.5×10^{-4} cm^2.V^{-1} s^{-1} could not be identified. By employing fluorescence detection for all the electropherograms, the presence of QDs and therefore the identification of GSH-QDs and ZnTCPPc-QDs peaks were confirmed. At the top of Fig. 2 is shown the electropherogram obtained with a fluorescence detector for the same ZnTCPPc-QDs sample, in which only the signal for ZnTCPPc-QDs is detected but not the interferences. Further exhaustive washing steps were performed with methanol and ethanol in order to avoid the presence of these impurities and to obtain accurate values for ζ-potential or equivalent sphere diameter. The purity of the samples was assessed by DAD-CZE. For subsequent studies in the CZE or TDA mode, the fluorescence detector was preferred.

Figure 3a shows the electropherograms obtained by CZE showing the ionic strength effect on the ZnTCPPc-QDs electrophoretic mobility (μ_E) in PB (pH 7.4). As expected, the absolute electrophoretic mobility values decrease with an increasing ionic strength due to counter-ions screening effect [35, 36]. The peak width of the CZE profiles increased on going from a relatively fine peak in 15 mM PB to larger profiles at ionic strengths between 25 and 100 mM probably due to electrophoretic dispersion. Indeed in these ζ-potential and ionic strength ranges, peak mobility dispersion should be increasingly sensitive to particle size distribution that may as well increase due to gradually enhanced interparticle interaction giving rise to aggregate formation at the highest ionic strength (IS) values. At 150 mM IS, a severe aggregation of ZnTCPPc-QDs was evidenced by the presence of repeatable spiky profiles. Electrophoretic profiles obtained by CE are narrower but comprised within the broad domain of electrophoretic mobilities determined by LDE (results not shown). This observation indicates a clear advantage of CE in terms of precision and sensitivity with respect to LDE.

Figure 3b presents ζ-potential values for ZnTCPPc-QDs either calculated from electrophoretic profiles displayed in Fig. 3a or derived from LDE measurements under the same analytical conditions. For this analysis, the hydrodynamic diameter at the corresponding IS was considered as described below. Calculated values from CE experiments indicate a decrease in absolute ζ-potential values when increasing ionic strength for ZnTCPPc-QDs (from −40.4 mV at 15 mM IS, to −12.4 mV at 150 mM IS). This observation is consistent with the differences in colloidal stability. Indeed, at high ζ-potential values, important electrostatic repulsions between nanoparticles occur, thereby preventing their aggregation in aqueous solutions. At 150 mM IS, the ζ-potential value is quite low, dropping below −20 mV which can explain the plain aggregation of the sample, as evidenced by spiky electrophoretic profiles (Fig. 3a). No significant variations in ζ-potential values could be evidenced by means of LDE across this ionic strength range (15–150 mM). This can be due to the presence of impurities, i.e., some traces of precursors used during Pc-QDs synthesis or functionalization, which is overcome by CE thanks to its resolving power. In the case of ZnMCPPc-QDs, no reliable ζ-potential values could be obtained due to the formation of large aggregates. The presence of carboxyl groups functionalizing the Pc ring makes the ZnTCPPc-QDs highly charged compared to the ZnMCPPc-QDs, in which one single carboxyl group is used to link the phthalocyanine to the GSH-QD. Reliable ζ-potential values were obtained for InTCPPc-QDs and AlTSPPc-QDs in SCB at pH 10.0 and 15 mM IS (−35.4 and −33.8 mV, respectively) by LDE.

Another determinant physicochemical parameter of the Pc-QDs is their size in aqueous solutions. An alternative technique to determine diffusion coefficients of solute molecules was presented long time ago by Taylor [33]. TDA using a capillary electrophoresis instrument appears to be a fast, simple, and reliable technique for performing diffusion coefficient (D) measurements of nanometric particle populations [19, 31,
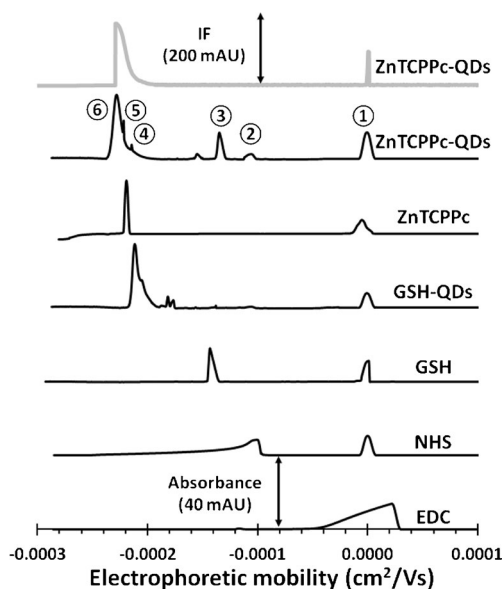

Fig. 2 Detection of impurities in the ZnTCPPc-QDs sample in pH 7.4 phosphate buffer solution at 15 mM. The peaks corresponds to (*1*) EOF marker, (*2*) NHS, (*3*) GSH, (*4*) GSH-QDs, (*5*) ZnTCPPc, and (*6*) conjugated ZnTCPPc-QDs. UV/vis detector at λ = 200 nm (*black lines*), and fluorescence detector (*gray line*). *IF*, fluorescence intensity.

Fig. 3 **a** Ionic strength effect on the electrophoretic mobility of QDs-ZnTCPPc in pH 7.4 phosphate buffer by using a fluorescence detector. *IF*, intensity of the fluorescence. **b** ζ-potential calculated from these electropherograms CE (*circles*) and compared with LDE (*triangles*)
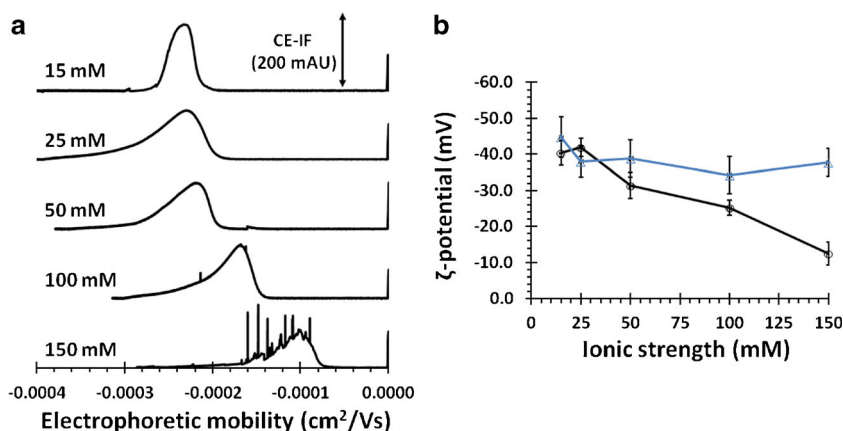
32]. In order to obtain apparent equivalent sphere diameter (d_h) values characterizing ZnTCPPc-QDs and ZnMCPPc-QDs, TDA was applied. Corresponding normalized taylorgrams obtained in front mode by applying a pressure drop of 30 mbar and an excitation wavelength of 488 nm for fluorescence detection are presented in Fig. 4 for various BGE ionic strengths. The mean residence time and the temporal variance σ^2 of each elution profiles were obtained by fitting the front concentration profile to the adequate equation [19]. Experimental profiles were very well fitted to the mathematical models. No significant variation in the retention time was detected in the taylorgrams for ZnTCPPc-QDs, indicating good robustness of the pressure system in addition to the absence of chromatographic retardation derived from
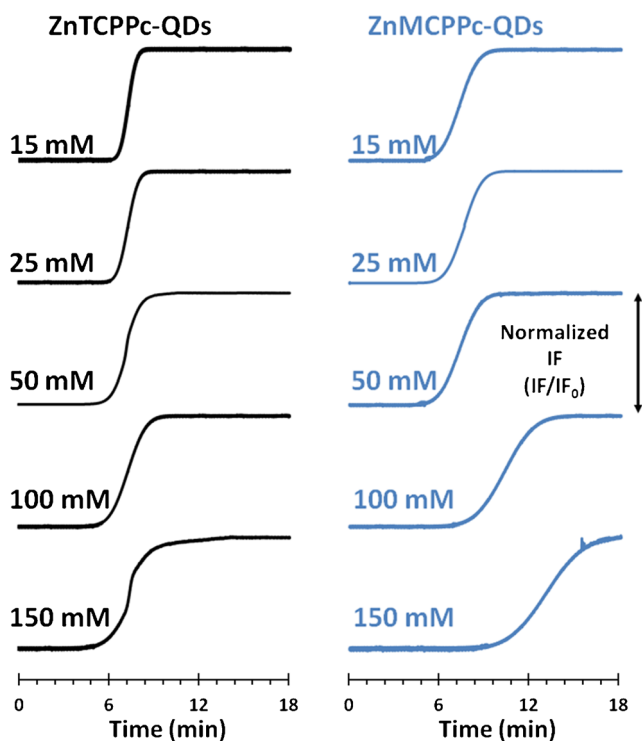
interactions between the NPs and the capillary wall. Otherwise, appreciable increase in the retention time and decrease in the slope were observed in the profiles obtained for ZnMCPPc-QDs. This difference can be due to the presence of larger ZnMCPPc-QDs aggregates than for ZnTCPPc-QDs.

The effect of single or poly-substitution of phthalocyanines (ZnMCPPc or ZnTCPPc) on the hydrodynamic diameter obtained by TDA was compared to the variations in the intensity weighted average particle hydrodynamic diameter (Z-average) determined by DLS (Table 1). In some cases, the DLS values are invalidated because they do not meet quality criteria (in range figure >83%), which can be due to several factors such as the presence of large or sedimenting particles, alteration of the refractive index (i.e., by sample fluorescence), or absorption of the incident laser light (colored samples) [37], all of them potentially present in our analyzed Pc-QDs samples. For DLS measurement, samples were diluted as far as possible using the same buffer at the corresponding ionic strength to suppress interparticle interactions and color or fluorescence effects, with the condition that QDs concentration has to be large enough to create sufficient scattered intensity at all scattering angles of interest [37]. The optimized concentrations were 0.15 and 0.2 mg/mL for ZnMCPPc-QDs and ZnTCPPc-QDs, respectively. Here again, the presence of ZnMCPPc-QDs aggregates could be detected, as the d_h was higher than 130 nm in all the ionic strength ranges. By comparing the results obtained by those two methodologies, data shown in Table 1 allow evidencing that TDA provides more precise results than DLS.

d_h values for ZnTCPPc-QDs and ZnMCPPc-QDs obtained by using TDA are constant for IS under 25 mM at around 28 and 125 nm, respectively (Tukey test ($p \leq 0.05$), $n = 4$ replicates). They increased with the IS for values higher than 50 mM. The higher d_h for ZnMCPPc-QDs than for ZnTCPPc-QDs can be explained by the lower surface charge density for the QD functionalized with one Pc (providing one carboxyl group) compared to the one functionalized with four Pc, leading to lower electrostatic repulsions between QDs and therefore to higher aggregation effect.


Fig. 4 Taylorgrams for size determination of ZnTCPPc-QDs and ZnMCPPc-QDs at various ionic strengths

Table 1 Ionic strength effect on the size parameters of (A) QDS-ZnTCPPc and (B) QDS-ZnMCPPc as obtained by DLS and CE-TDA in pH 7.4 phosphate buffer solution ($n = 4$)

Ionic strength (mM)	Type of conjugated	Hydrodynamic diameter by DLS (nm)	PDI	Diffusion coefficient by TDA ($\times 10^{-12}$ m^2/s)	Hydrodynamic diameter by TDA (nm)
15 mM	A	27.1 ± 14.0	0.158	18.2 ± 5.26	27.0 ± 7.8
	B	134.1 ± 65.8	0.214	3.82 ± 0.46	128.2 ± 15.4
25 mM	A	60.4 ± 21.0	0.234	16.6 ± 6.39	29.6 ± 11.4
	B	103.8 ± 58.4	0.342	3.96 ± 0.42	123.8 ± 13
50 mM	A	172.2 ± 49.2	0.245	6.36 ± 0.46	77.0 ± 5.6
	B	166.9 ± 48.9	0.219	3.00 ± 0.25	163.4 ± 13.8
100 mM	A	181.4 ± 38.0	0.234	3.74 ± 0.27	131.2 ± 9.4
	B	179.5 ± 37.7	0.239	1.98 ± 0.11	248.2 ± 13.9
150 mM	A	145.2 ± 46.4	0.353	2.81 ± 0.22	175.4 ± 14.4
	B	161.8 ± 28.1	0.417	1.56 ± 0.13	313.2 ± 27.0

Similar d_h values were obtained by means of DLS measurements, with a lower precision (higher standard deviation values) than TDA (Table 1). Equal QDS-ZnTCPPc or QDS-ZnMCPPc concentrations were used for both techniques. Both QDs presented an increase in their d_h while increasing the IS. The differences in the d_h values from CE and DLS can be due to the interferences in the light scattering measurements caused by the inherent fluorescence or color presence of the QDs. With DLS, the particle size is not directly measured, but is calculated from the measured Brownian motion (diffusion coefficient) of the sample [38, 39]. Accuracy in DLS is also reliant on knowing the refractive index of the nanoparticles and the viscosity and refractive index of the dispersant. The assumption of a quantum dot refractive index of 2.550 [29] and a dispersant refractive index of 1.3325 with a viscosity of 0.8872 cP was made consistently across all the dispersions. Results obtained by this technique are usually reported as the mean size, the z-average diameter, which is calculated based on the diffusion coefficient derived from the correlation function [29]. In the cases in which the intensity DLS plots contained more than one peak (due to Pc-QDs aggregation), we are not reporting the z-average value; instead we report the diameter corresponding to scattering peak that has the highest relative weight when considering the number-size distribution. By considering the effect of multi-substituents in phthalocyanines, we expected to obtain good dispersion and colloidal stability of the AlTSPPc-QDs and InTCPPc-QDs in phosphate buffer solution under the same conditions as in the case of ZnTCPPc-QDs. When analyzing by DLS and in 15 mM phosphate buffer (6.5–8.0 pH range) or sodium carbonate buffer (9.0–10.5 pH range) (Fig. 5), AlTSPPc-QDs and InTCPPc-QDs aggregation was identified in the 6.5 to 9.0 pH range, whereas good dispersion was observed for pH values higher than 9.0. By comparison, a good colloidal stability was obtained for ZnTCPPc-QDs at pH values higher than pH 7.4. The presence of the Cl- and OH-substituents bounded to the metallic center of the

phthalocyanines in AlTSPPc-QDs and InTCPPc-QDs, respectively, enhance interparticle interactions at pH ≤9.0. These chloride and hydroxyl groups can indeed interact with other molecules, leading to aggregation at pH values lower than 9.5. This observation gives clues for the analysis and design of new conjugated QDs, but in general for functionalized-NPs.

As conclusions, this study shows the efficiency and powerfulness of the CZE method complemented with TDA-CE for the characterization of the colloidal stability of Pc-QDs, and provides an important reference on the study and preparation of these functionalized QDs. Electropherograms and taylorgrams can be used for the ζ-potential and size analysis of NPs. In addition the Pc-QD characterization by CE is performed without any extensive purification and provides in the same run the identification of impurities in the samples. The results were compared and complemented by screening LDE and DLS methods. The presence of multi-substituents in the phthalocyanine ring enhances the colloidal dispersion of the Pc-QDs by means of the creation of electrostatic repulsion of the functional groups attached to the aromatic rings in the
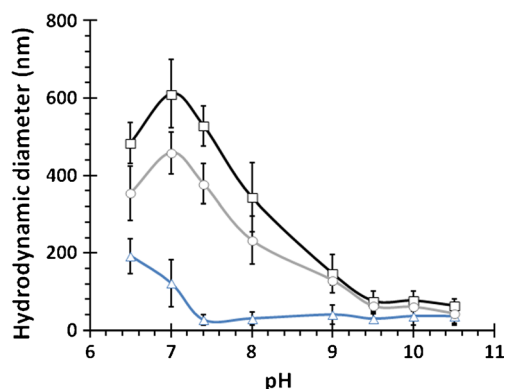
Fig. 5 pH effect on the hydrodynamic diameter of phthalocyanine functionalized QDs. QDS-InTCPPc (*squares*), QDs-AlTSPc (*circles*), and QDs-ZnTCPPc (*triangles*) by DLS in phosphate buffer solution (pH 6.5–8.0) and sodium carbonate buffer (pH 9.0–10.5) at 15 mM

phthalocyanine. However, the hydroxyl and chloride groups bounded to the metallic center of the phthalocyanine have an antagonist effect in colloidal stability, and then aggregation is observed at values lower than pH 9.0. As the CZE methodology allows for separation of the different components of the sample, it presents the main advantage of providing more accurate determination than with the classical methods. As CE provides information on QDs in various solutions, among which physiological ones, this methodology seems therefore very important for the accurate quantitative QDs characterization before their use for biomedical applications. Due to the photophysical properties of QDs, which origin interferences in the LDE and DLS measures, a non-optical method as CE became the most interesting technique for the characterization of their colloidal properties in physiologically relevant aqueous solutions.

Compliance with ethical standards

Conflict of interest The authors declare that they have no conflict of interest.

References

1. Breger J, Delehanty JB, Medintz IL. Continuing progress toward controlled intracellular delivery of semiconductor quantum dots. Wiley Interdiscip Rev Nanomed Nanobiotechnol. 2015;7(2):131–51. doi:10.1002/wnan.1281.

2. Mussa Farkhani S, Valizadeh A. Review: three synthesis methods of CdX (X = Se, S or Te) quantum dots. IET Nanobiotechnol. 2014;8(2):59–76. doi:10.1049/iet-nbt.2012.0028.

3. Volkov Y. Quantum dots in nanomedicine: recent trends, advances and unresolved issues. Biochem Biophys Res Commun. 2015;468(3):419–27. doi:10.1016/j.bbrc.2015.07.039.

4. Maysinger D, Ji J, Hutter E, Cooper E. Nanoparticle-based and bioengineered probes and sensors to detect physiological and pathological biomarkers in neural cells. Front Neurosci. 2015;9:480. doi:10.3389/fnins.2015.00480.

5. Petryayeva E, Algar WR, Medintz IL. Quantum dots in bioanalysis: a review of applications across various platforms for fluorescence spectroscopy and imaging. Appl Spectrosc. 2013;67(3):215–52. doi:10.1366/12-06948.

6. Lucky SS, Soo KC, Zhang Y. Nanoparticles in photodynamic therapy. Chem Rev. 2015;115(4):1990–2042. doi:10.1021/cr5004198.

7. Oluwole DO, Nyokong T. Physicochemical behavior of nanohybrids of mono and tetra substituted carboxyphenoxy phthalocyanine covalently linked to GSH–CdTe/CdS/ZnS quantum dots. Polyhedron. 2015;87:8–16. doi:10.1016/j.poly.2014.10.024.

8. Oluwole DO, Nyokong T. Comparative photophysicochemical behavior of nanoconjugates of indium tetracarboxyphenoxy phthalocyanines covalently linked to CdTe/ZnSe/ZnO quantum dots. J Photoch Photobio A. 2015;312:34–44. doi:10.1016/j.jphotochem.2015.07.009.

9. Oluwole DO, Britton J, Mashazi P, Nyokong T. Synthesis and photophysical properties of nanocomposites of aluminum tetrasulfonated phthalocyanine covalently linked to glutathione capped CdTe/CdS/ZnS quantum dots. Synth Met. 2015;205:212–21. doi:10.1016/j.synthmet.2015.04.015.

10. Li L, Huh KM. Polymeric nanocarrier systems for photodynamic therapy. Biomater Res. 2014;18.

11. Lopez-Serrano A, Olivas RM, Landaluze JS, Camara C. Nanoparticles: a global vision. Characterization, separation, and quantification methods. Potential environmental and health impact. Anal Methods. 2014;6(1):38–56. doi:10.1039/C3AY40517F.

12. Ban E, Yoo YS, Song EJ. Analysis and applications of nanoparticles in capillary electrophoresis. Talanta. 2015;141:15–20. doi:10.1016/j.talanta.2015.03.020.

13. Trapiella-Alfonso L, d'Orlyé F, Varenne A. Recent advances in the development of capillary electrophoresis methodologies for optimizing, controlling, and characterizing the synthesis, functionalization, and physicochemical, properties of nanoparticles. Anal Bioanal Chem. 2016:1-7. doi:10.1007/s00216-015-9236-7.

14. Li YQ, Wang HQ, Wang JH, Guan LY, Liu BF, Zhao YD, et al. A highly efficient capillary electrophoresis-based method for size determination of water-soluble CdSe/ZnS core-shell quantum dots. Anal Chim Acta. 2009;647(2):219–25. doi:10.1016/j.aca.2009.06.004.

15. Stewart DTR, Celiz MD, Vicente G, Colón LA, Aga DS. Potential use of capillary zone electrophoresis in size characterization of quantum dots for environmental studies. Tr Anal Chem. 2011;30(1):113–22. doi:10.1016/j.trac.2010.10.005.

16. Sang F, Huang X, Ren J. Characterization and separation of semiconductor quantum dots and their conjugates by capillary electrophoresis. Electrophoresis. 2014;35(6):793–803. doi:10.1002/elps.201300528.

17. Radko SP, Chrambach A. Separation and characterization of sub-mu m- and mu m-sized particles by capillary zone electrophoresis. Electrophoresis. 2002;23(13):1957–72. doi:10.1002/1522-2683(200207)23:13<1957::aid-elps1957>3.0.co;2-i.

18. d'Orlye F, Varenne A, Georgelin T, Siaugue JM, Teste B, Descroix S, et al. Charge-based characterization of nanometric cationic bifunctional maghemite/silica core/shell particles by capillary zone electrophoresis. Electrophoresis. 2009;30(14):2572–82. doi:10.1002/elps.200800835.

19. d'Orlyé F, Varenne A, Gareil P. Determination of nanoparticle diffusion coefficients by Taylor dispersion analysis using a capillary electrophoresis instrument. J Chromatogr A. 2008;1204(2):226–32. doi:10.1016/j.chroma.2008.08.008.

20. Wang YH, Wang L. Defect states in Nd^{3+}-doped $CaAl_2O_4 : Eu^{2+}$. J Appl Phys. 2007;101(5). doi:10.1063/1.2435822.

21. Fourest B, Hakem N, Guillaumont R. Characterization of colloids by measurement of their mobilities. Radiochim Acta. 1994. p. 173.

22. Huang X, Weng J, Sang F, Song X, Cao C, Ren J. Characterization of quantum dot bioconjugates by capillary electrophoresis with laser-induced fluorescent detection. J Chromatogr A. 2006;1113(1-2):251–4. doi:10.1016/j.chroma.2006.02.087.

23. Trapiella-Alfonso L, Ramírez-García G, d'Orlyé F, Varenne A. Electromigration separation methodologies for the characterization of nanoparticles and the evaluation of their behaviour in biological

systems. Tr Anal Chem. 2016;84(Part A):121–30. doi:10.1016/j.trac.2016.04.022.

24. Ramirez-Garcia G, d'Orlye F, Gutierrez-Granados S, Martinez-Alfaro M, Mignet N, Richard C, et al. Functionalization and characterization of persistent luminescence nanoparticles by dynamic light scattering, laser Doppler and capillary electrophoresis. Colloid Surface B. 2015;136:272–81. doi:10.1016/j.colsurfb.2015.09.022.

25. Rivera Gil P, Oberdörster G, Elder A, Puntes V, Parak WJ. Correlating physico-chemical with toxicological properties of nanoparticles: the present and the future. ACS Nano. 2010;4(10):5527–31. doi:10.1021/nn1025687.

26. Powers KW, Brown SC, Krishna VB, Wasdo SC, Moudgil BM, Roberts SM. Research strategies for safety evaluation of nanomaterials. Part VI. Characterization of nanoscale particles for toxicological evaluation. Toxicol Sci. 2006;90(2):296–303. doi:10.1093/toxsci/kfj099.

27. Nam J, Won N, Bang J, Jin H, Park J, Jung S, et al. Surface engineering of inorganic nanoparticles for imaging and therapy. Adv Drug Deliv Rev. 2013;65(5):622–48. doi:10.1016/j.addr.2012.08.015.

28. Sperling RA, Parak WJ. Surface modification, functionalization and bioconjugation of colloidal inorganic nanoparticles. Philos T Roy Soc A. 2010;368(1915):1333–83. doi:10.1098/rsta.2009.0273.

29. Hondow N, Brydson R, Wang P, Holton MD, Brown MR, Rees P, et al. Quantitative characterization of nanoparticle agglomeration within biological media. J Nanopart Res. 2012;14(7):1–15. doi:10.1007/s11051-012-0977-3.

30. Milanova D, Chambers RD, Bahga SS, Santiago JG. Electrophoretic mobility measurements of fluorescent dyes using on-chip capillary electrophoresis. Electrophoresis. 2011;32(22):3286–94. doi:10.1002/elps.201100210.

31. Pyell U, Jalil AH, Pfeiffer C, Pelaz B, Parak WJ. Characterization of gold nanoparticles with different hydrophilic coatings via capillary electrophoresis and Taylor dispersion analysis. Part I: determination of the zeta potential employing a modified analytic approximation. J Colloid Interface Sci. 2015;450:288–300. doi:10.1016/j.jcis.2015.03.006.

32. Pyell U, Jalil AH, Urban DA, Pfeiffer C, Pelaz B, Parak WJ. Characterization of hydrophilic coated gold nanoparticles via capillary electrophoresis and Taylor dispersion analysis. Part II: determination of the hydrodynamic radius distribution—comparison with asymmetric flow field-flow fractionation. J Colloid Interface Sci. 2015;457:131–40. doi:10.1016/j.jcis.2015.06.042.

33. Taylor G. Dispersion of soluble matter in solvent flowing slowly through a tube. P Roy Soc Lond A Mat. 1953;219(1137):186–203. doi:10.1098/rspa.1953.0139.

34. Aris R. On the dispersion of a solute in a fluid flowing through a tube. P Roy Soc Lond A Mat. 1956;235(1200):67–77. doi:10.1098/rspa.1956.0065.

35. Wu L, Zhang J, Watanabe W. Physical and chemical stability of drug nanoparticles. Adv Drug Deliv Rev. 2011;63(6):456–69. doi:10.1016/j.addr.2011.02.001.

36. Kuzovkov VN, Kotomin EA. Static and dynamic screening effects in the electrostatic self-assembly of nano-particles. Phys Chem Chem Phys. 2014;16(46):25449–60. doi:10.1039/C4CP02448F.

37. Brar SK, Verma M. Measurement of nanoparticles by light-scattering techniques. TrAC T Anal Chem. 2011;30(1):4–17. doi:10.1016/j.trac.2010.08.008.

38. Hoo CM, Starostin N, West P, Mecartney ML. A comparison of atomic force microscopy (AFM) and dynamic light scattering (DLS) methods to characterize nanoparticle size distributions. J Nanopart Res. 2008;10(1):89–96. doi:10.1007/s11051-008-9435-7.

39. Sapsford KE, Tyner KM, Dair BJ, Deschamps JR, Medintz IL. Analyzing nanomaterial bioconjugates: a review of current and emerging purification and characterization techniques. Anal Chem. 2011;83(12):4453–88. doi:10.1021/ac200853a.